Research Square

Preprints are preliminary reports that have not undergone peer review.
They should not be considered conclusive, used to inform clinical practice,
or referenced by the media as validated information.

Multi-omics integration of malignant peripheral nerve sheath tumors nominates therapies based on chromosome 8q status

Belinda B. Garana
Pacific Northwest National Laboratory
Jiawan Wang
Johns Hopkins University School of Medicine
Simge Acar
Washington University of St. Louis
Chelsea Hutchinson-Bunch
Pacific Northwest National Laboratory
Gorkem Oztosun
Washington University of St. Louis
Stavriani C. Makri
Johns Hopkins University School of Medicine
Dana C. Borcherding
Washington University of St. Louis
Ying Zou
Johns Hopkins University School of Medicine
Marina A. Gritsenko
Pacific Northwest National Laboratory
Paul D. Piehowski
Pacific Northwest National Laboratory
Christine A. Pratilas
Johns Hopkins University School of Medicine
Angela C. Hirbe
Washington University of St. Louis
Sara J.C. Gosline
sara.gosline@pnnl.gov

Pacific Northwest National Laboratory

Article

Keywords: MPNST, proteomics, copy number alteration, EGFR, PLK1

Posted Date: April 28th, 2026

DOI: https://doi.org/10.21203/rs.3.rs-9097791/v1

License: This work is licensed under a Creative Commons Attribution 4.0 International License.
Read Full License

Additional Declarations: No competing interests reported.

Abstract

Chromosome 8q (chr8q) copy number gain is associated with high-grade transformation in malignant peripheral nerve sheath tumors (MPNST), an aggressive soft tissue sarcoma. To identify potential treatments for patients with chr8q gain, we leveraged our library of MPNST patient-derived xenografts (PDX) and collected global proteomics and phosphoproteomics measurements for six of these models. We integrated these data with transcriptomics and copy number data to identify the multiomics networks altered by chr8q status, which were then used to nominate drug candidates.

Our results identify the chr8q gene *MYC* as a key driver of chr8q gain-related effects and suggest that these samples could be targeted with PLK1 inhibitors, while MPNSTs without *MYC* gain might benefit more from EGFR inhibition. We tested this hypothesis through *in vitro* validation, showing that multiomic integration can identify drug therapies to selectively target tumors based on genetic aberration, even in rare cancers where sample size is small.

Background

Malignant peripheral nerve sheath tumors (MPNST) are aggressive soft-tissue sarcomas with poor prognosis. Only 20–50% of patients over twenty years of age will survive five years from diagnosis.[1] MPNST are usually treated with surgery, with or without chemotherapy and/or radiotherapy. As many as seventy percent of patients develop metastases for which systemic treatment is the only option but is rarely able to achieve durable clinical benefit.[2] To date, no effective targeted therapies have been successful in clinical trials for MPNST, and the median progression free survival (PFS) observed in these trials has been less than two months.[3–5]

Loss of neurofibromin (NF1) and consequent hyperactivation of RAS effector pathways is a key genomic feature required for MPNST development, but other genomic events drive malignant transformation and may confer a more aggressive phenotype [1,6,7] To advance our understanding of biological features expressed by the complex genetic landscape of MPNST, and to offer models suitable for drug testing, we and others have developed patient-derived xenograft (PDX) models of NF1-MPNST [1,8–11] in immunodeficient mice. Using these models, our group found that chromosome 8q (chr8q) gain is associated with high-grade transformation in MPNST and inferior overall survival in 262 patient samples with soft-tissue sarcoma.[8] The study now presented herein characterizes the molecular and proteomic changes that accompany chr8q gain in these MPNST-PDX models to identify novel targeted treatments for this aggressive subset.

Proteomics offers valuable information about proteins which are directly targetable with small molecule therapeutics, and protein activity through post-translational modifications including phosphorylation. By understanding the proteomic changes driving the aggressive phenotype associated with chr8q gain in MPNST, we posited that we would identify actionable targets with existing, approved drugs, the activity of which has not previously been tested in MPNST. To examine the proteomic differences in these NF1-

MPNST models, we collected liquid chromatography tandem mass spectrometry-based (LC-MS/MS) proteomics using six PDX models. We then integrated the proteomics measurements with copy number data derived from whole genome sequencing and RNA sequencing to identify trends in protein and gene expression associated with chr8q copy number. We employed correlation-based analyses to identify several pathways differentially regulated in MPNST PDX based on chr8q gain and potential drivers which may be coordinating these changes. Additionally, we interrogated the publicly available Cancer Cell Line Encyclopedia for 327 adherent cancer cell lines to identify potential drug candidates. By integrating these multi-omics data sets, we nominated drug candidates to uniquely target chr8q gain or diploid tumors, and then validated these findings in patient-derived cell lines.

Results

Multi-omics analysis illustrates dramatic molecular differences associated with chr8q gain

To identify signaling changes associated with chr8q copy number alteration and to characterize the molecular milieu across the heterogeneous tumor landscape, we leveraged six previously reported PDX[1,8–11] (Fig. 1A-B) and collected LC-MS/MS measurements of both the global proteome and phosphoproteome using the samples as described in Methods. From these measurements, we identified 9,013 proteins and 29,545 phospho-sites that were present in at least 50% of the samples measured (Table S1-2). To examine the association between chr8q gain and RNA, protein, and phospho-peptide expression, we leveraged existing copy number and RNA-Seq data from these six PDX as well as copy number and RNASeq measurements from other previously published PDX: JH-2-055b, MN-3, WU-536, WU-561, JH-2-023, WU-356, WU-386, WU-436, JH-2-031, and WU-225 [1,8–11].

We hypothesized that molecular features that were positively correlated with chr8q status (Fig 1B) would be involved in signaling pathways active in chr8q amplified samples, while those negatively correlated would represent signaling pathways more active in chr8q diploid samples. Therefore, we measured Spearman rank-based correlations between chr8q copy number and gene, protein, and phosphosite expression, and then used these correlation values as input into our gene enrichment statistics to identify over-represented pathways in both the chr8q gain group and the diploid group. These correlations, depicted in Fig. 1C (and Table S3), can then be evaluated for statistical significance. We then filtered the features to identify those that have an absolute correlation >0.75 and an adjusted p-value < 0.05 (see Methods).

Using this correlation-based approach, we found 1630 (2.19%) transcripts, 208 (2.31%) proteins, and 439 (1.12%) phospho-sites representing 319 proteins to be significantly correlated with chr8q status (Fig. 1D-E; Table S3). Transcripts showed more statistically significant positive correlation overall (Figure 1C, top panel), consistent with the established role of MYC (located on chr8q24) in regulating to overall increase in transcript abundance[12]. Out of the top correlated features based on absolute Spearman

correlation estimates across three levels of biological data, we found 103 transcripts, 10 proteins, and 6 phosphosites that are associated with genes that physically reside on chr8q (Fig 1C, darker lines, Table S3), meaning that most associations with chr8q are not simply direct measurements of chr8q gain but instead downstream effects of chr8q. This analysis demonstrates that chr8q gain is associated with nontrivial changes in transcriptomic, proteomic, and phosphoproteomic expression.

To determine if this correlation approach could indeed identify enriched pathways via rank statistics, we used Gene Set Enrichment Analysis with a positional gene list to ask if gene-based copy number data was enriched on chromosome 8. The results, depicted in Fig. 1F and Table S4, show that most of the segments on chr8 were enriched in positively correlated gene copy numbers as expected. Specifically, all seven segments of chr8q measured were significantly positively enriched (i.e., had greater copy number with higher median chr8q copy number), with chr8q24 (where the oncogene *MYC* is located) being the most strongly enriched (NES = 5.18, p < 1E-3, FDR < 1E-3) (Table S4). One chr8p segment was significantly negatively enriched (chr8p23, NES = -2.2, p < 1E-3, FDR = 1.20E-5) out of five chr8p segments quantified, meaning genes located on these chr8p segments tended to have lower copy number in samples with higher copy numbers of genes located on chr8q [13]. However, three of the five chr8p segments were significantly positively enriched, following the trend of the long arm of chr8 (q). This enrichment of chr8q confirms that our rank-based correlation-enrichment approach can reflect changes in line with chr8q copy number.

Enrichment results show distinct pathway activation patterns with chr8q gain

To quantify pathway-level effects of variation in chr8q, we performed gene set enrichment analysis[14] (Table S4 and Fig. 2) using the feature rankings imposed by correlations between median chr8q copy number and expression. We posited that positively enriched pathways indicate pathways with higher activity in samples with higher chr8q copy number and negatively enriched pathways have higher expression in samples with lower chr8q copy number. These results, depicted in Fig. 2A, identify 11 out of 50 Hallmark pathways significantly enriched at the protein level and 18 out of 50 at the RNA level, with 3 pathways in common and significantly positively enriched: MYC targets, E2F targets, and G2M checkpoint (Fig. 2A). Increased activity of MYC with chr8q gain is expected because MYC is located on chr8 itself (specifically chr8q24.21).[15] We also used enrichment analysis to look for transcription factors using RNA-seq correlations and the transcription factor-target gene list and kinases using phosphoproteomics with a kinase-substrate list (Fig. 2B, Table S4-5). This analysis suggests 260 transcription factors out of 470 evaluated are significantly more active with higher chr8q copy number but transcription factors TFAM and HMCES may be less active in samples with neutral chr8q copy number (Fig. 2B). Additionally, three out of 182 kinases evaluated (NEK1, MOK, PRKG2) were predicted to be less active in samples with higher chr8q copy number while five kinases were predicted to be more active (Fig. 2C).

We then searched for links between MYC, the presumed regulator of these changes, and the proteins, transcription factors, and targets identified in then enrichment analysis of positively and negatively correlated features. To identify these links we used the STRING physical interaction database[16] to identify physical interactions between proteins encoded by genes on chromosome 8q and proteins, transcription factors, and kinases that are positively or negatively correlated with chr8q status (Table S6). We found ten proteins encoded by chr8q genes that were directly interacting with protein regulators and asked if they played a central role in the physical network connecting the associated features using the network centrality statistic. The results, depicted in Fig. 2D, show the centrality of the 10 genes in both the positively correlated (red) and negatively correlated (blue) networks. As expected, MYC was the most central, particularly in the network of up-regulated features, suggesting it is highly relevant to the features identified in the correlation analysis. Metabolic proteins MRPL15 and MRPS28 were most central in networks active in samples with less chr8q amplification, corresponding with the increased apoptosis pathway enriched in these same samples in Fig. 2A. Together, these results suggest that chr8q gain drives increased MYC activity that leads to network level changes at the transcriptional, protein, and phospho-protein levels.

Drug sensitivity analysis nominates potential targets based on chr8q status

To complement our feature-based search of drug targets, we employed a data-driven approach that leverages published drug sensitivity data across a panel of 327 adherent cancer cell lines (see Methods, Table S7) to identify potentially drug sensitivities that are unique to MPNST populations segregated by chr8q status. Specifically, we ranked each cell line by how similar it was to each our chr8q signatures (derived using transcriptomics or proteomics, see Methods). These rankings were then correlated with drug sensitivity scores (in this case, area under the dose response curve, or AUC), with negative correlations suggesting that MPNSTs with higher chr8q copy number may be more sensitive to the drug of interest, and positive correlations indicating that chr8q-diploid MPNST may be more sensitive. The result is a set of scores for each drug based on the extent to which cell line drug sensitivities correlate with the MPNST chr8q status, which we can use to both rank drugs based on predicted sensitivity as well as identify classes that are over-represented using enrichment statistics.

Out of 1,448 drugs in the PRISM repurposing database,[17] 83 had sensitivity correlated with expression of protein signatures and 94 were correlated with expression of transcript signatures (adjusted p-value < 0.05). Out of the top 5 correlated drugs based on absolute Pearson correlation, the top drugs predicted to be selective active against chr8q-diploid MPNST are EGFR inhibitors (Fig. 3A) and the top drug predicted to be selectively active against MPNST with chr8q gain include two PLK1 inhibitors (Fig. 3B). The full results are in Table S6. To see if the results from Fig 3A translated to other drugs within the same drug class, we grouped all drugs by assigned drug mechanism, and then used additional enrichment statistics to identify which mechanisms were enriched with negative drug-chr8q correlations

and which were enriched with positive drug-chr8q correlations. Drug mechanisms with a negative NES are predicted to be more effective against MPNSTs with higher chr8q copy number whereas those with a positive NES may be more effective against chr8q-diploid MPNSTs. Of the 83 drug mechanisms evaluated, 14 were predicted to be more effective in chr8q gain (negative NES score, Fig. 3C), and 9 were predicted to be more effective with lower amounts of chr8q gain (positive NES score, Fig. 3C). More importantly, we found enrichment among polo-like kinase (PLK) inhibitors, predicted to be more effective in chr8q gain samples, and EGFR inhibitors, predicted to be more effective in samples with lower levels of chr8q suggesting that these two classes of drugs could be effective in the two MPNST populations.

To examine if the predicted drug targets had existing links to MYC or the features we identified to be correlated with chr8q status (in Fig. 2), we employed a network approach. Specifically, we sought to identify physical interactions between enriched kinases and transcription factors, correlated proteins, MYC (which we hypothesize may drive the effects of chr8q gain), and two putative drug targets EGFR and PLK1. For the drug target EGFR, we explored connections between MYC, proteins with expression negatively correlated with median chr8q copy number, the three negatively enriched kinases, and the negatively enriched transcription factors. We also searched for connections between the drug target PLK1 and MYC, proteins with expression positively correlated with median chr8q copy number, positively enriched kinases, and positively enriched transcription factors. We identified thirteen downregulated proteins known to directly interact with EGFR and four proteins linking EGFR to MYC (Fig. 3D). Among the correlated features, we found five upregulated proteins and three upregulated transcription factors known to directly interact with PLK1 and including a correlated protein linking PLK1 to MYC (Fig. 3E). The fact that the proteins identified by our multi-omics analysis identified direct physical interactions between MYC and drug targets shows additional evidence to suggest that PLK1 and EGFR inhibitors might selectively target MPNST in a chr8q copy number-dependent fashion.

Fluorescence in situ hybridization (FISH) determines chr8 and MYC copy number status across NF1-MPNST cell lines.

To validate the differential drug response suggested by our multi-omics analysis, we sought out nine existing NF1-MPNST cell lines to determine if their chr8q status determined their drug response. We first measured chr8/*MYC* copy number status of nine NF1-MPNST cell lines, including the newly established JH-2-055d cell line (corresponding to the same patient from which the PDX JH-2-055b was derived, but at a subsequent recurrence), using fluorescence in situ hybridization (FISH; Tables 1 & S8 and Fig. 4A-C) with probes for the centromere of chromosome 8 (cep8), *MYC* (chr8q24), and *IGH* (chr14q32). Within this nine cell-line panel, six (67%) cell lines exhibited gain in chr8 (3 or more copies of the centromere of chr8), and eight (89%) showed gain in *MYC*/8q24 in over 50% of cells. Only one cell line (JH-2-055d) was *MYC* diploid and three were chr8 diploid (JH-2-055d, NF10.1, and ST8814, Fig. 4C). Given the high prevalence of chr8q gain in MPNST, we are not aware of any other chr8q diploid MPNST cell lines. Specifically, of MPNST cell lines with chr8 gain, most (5 out of 6) had gain in 100% of cells except NF90.8 which had chr8 gain in 84% of cells. Chr8 diploid JH-2-055d revealed chr8 gain in just 11% of cells. Similarly, *MYC* gain occurred in 100% of cells for most cell lines (7 out of 9) tested except for

NF90.8 which had *MYC* gain in 98% of cells and *MYC* diploid JH-2-055d where again just 11% of cells had *MYC* gain. For NF11.1, there was non-specific binding observed for the cep8 probe so it could not be distinguished whether NF11.1 had either 3 or 6 copies of centromere 8 but 100% of NF11.1 cells still met the criteria for chr8 gain with at least 3 copies of chr8 (Fig. 4A). We integrated the FISH copy number analysis of chr8 and *MYC* in the current study and molecular alterations in other key genomic drivers of MPNST from our previous report[18] (Fig. 4B), which showed that chr8q gain alongside loss of *NF1*, *CDKN2A,* and PRC2 components *SUZ12* and *EED* are common genomic events in MPNST. Notably, the chr8q arm gain was observed more frequently than a gain of the entire chr8 centromere region on this panel of NF1-MPNST cell lines (Fig. 4C). These results are summarized in Table 1 and were then used to stratify cell lines for investigation of drug response, particularly validation of drug candidates nominated above by proteogenomics coupled with drug mechanism analyses.

Table 1. Chr8 and *MYC* copy number determined by FISH

Cell line	**Chr8 gain** in ≥ 50% of cells	***MYC* / 8q24 gain** in ≥ 50% of cells
ST8814	No	100%
NF90.8	84%	98%
S462	100%	100%
NF10.1	No	100%
NF11.1	100%	100%
JH-2-002	100%	100%
JH-2-055d	No	No
JH-2-079c	100%	100%
JH-2-103	100%	100%

PLK and EGFR are potential targets depending on MYC status

Drug sensitivity analysis of the PRISM drug repurposing datasets[17] predicted the preferential activity of the PLK1 inhibitors BI-2536 and volasertib (NMS-1286937) against MPNST with chr8q gain, and the selective activity of the EGFR inhibitors poziotinib and pelitinib against chr8q-diploid MPNST (Fig. 3B-C). Given the lack of efficacy and/or toxicity concerns about these two pan-ErbB inhibitors in many other cancers[19–22], and the implication of altered EGFR signaling in a subset of MPNST,[23–25] we focused our analysis on more specific EGFR inhibitors instead, specifically the two FDA-approved EGFR inhibitors erlotinib (1st generation) and osimertinib (3rd generation).

To assess the efficacy of PLK1 and EGFR inhibitors on MPNST, we treated nine NF1-MPNST cell lines with PLK1 inhibitors volasertib (clinical stage) and BI-2536 (preclinical compound) and EGFR inhibitors erlotinib and osimertinib for five days (Table S9 and Fig. 5). We grouped the cell lines in Table 1 by chr8 and *MYC* status and compared the difference in cell viability across increasing doses of drug. First, we found chr8 gain lines (all except JH-2-055d) to be more sensitive to PLK1 inhibitors based on IC50 (Fisher combined p = 1.65E-2; p = 5.85E-2 for BI-2536 and p = 4.00E-2 for volasertib) than those without chr8 gain (Fig. 5A & C). Additionally, we found that the chr8 diploid lines were more sensitive to EGFR inhibitors (Fisher combined p = 2.82E-2; p = 1.13E-1 for erlotinib and p = 3.87E-2 for osimertinib) than chr8 gain based on IC50 values (Fig. 5B &D).

Given our hypothesis that the effects of chr8q gain are mainly driven by MYC, we repeated these statistical tests based on the gain status of *MYC* alone instead of all of chr8. Using this approach, we found the difference in IC50 was greater based on *MYC* status than chr8 status: *MYC* gain lines were more sensitive to PLK inhibitors (Fisher combined p = 8.98E-29; p = 1.40E-2 for BI-2536 and p = 9.18E-29 for volasertib; Fig. 5A & C) whereas our *MYC* diploid line was more sensitive to EGFR inhibitors (Fisher combined p = 3.99E-7; p = 3.15E-4 for erlotinib and p = 6.79E-5 for osimertinib; Fig. 5B & D). These *in vitro* data suggests that PLK1 and EGFR may be targetable vulnerabilities in MPNST depending on *MYC* status.

Methods

MPNST PDX samples

MPNST PDX samples were generated in our laboratories at Johns Hopkins University (JH; Baltimore, MD, USA) and Washington University St. Louis (WU, St. Louis, MO) from biospecimens collected during surgical resection from patients with NF1 as previously published.[9,11] Material was collected under Institutional Review Board–approved protocols and all patients provided written informed consent.

LC-MS/MS proteomic measurement of MPNST PDX samples

Proteomics sample preparation and data processing followed protocols developed under the CPTAC consortium.[26–28] mzRefinery was used to process all Thermo RAW files to correct for mass calibration errors before spectra were searched with MS-GF + v9881[29–31] to match against the RefSeq human protein sequence database, release version 38 (https://www.ncbi.nlm.nih.gov/datasets/genome/GCF_000001405.26/). Static carbamidomethylation (+57.0215 Da) on Cys residues, TMT modification (+229.1629 Da) on the peptide N terminus and Lys residues, and dynamic oxidation (+15.9949 Da) on Met residues were considered using MS-GF +. Phosphopeptide enrichment was performed using the Agilent AssayMap Phosphopeptide enrichment platform with Fe(III)-NTA cartidges (https://www.agilent.com/cs/library/applications/5991-6073EN.pdf?

srsltid=AfmBOopbnJkl5BspPffXibmWt24zkX7z9q6Ov2NFb65Rkenm4tz2EBvi).First, peptide fractions were resuspended in 200 ul in 80% acetonitrile (ACN)/0.1% TFA then centrifuged at 6,000g for 5 minutes to remove insoluble material. Samples were transferred to polypropylene 96-well plates. Priming buffer for the cartridges consisted of 50% ACN/0.1% TFA, 80% ACN/0.1% TFA was used as the equilibration buffer and internal cartridge wash buffer, and the elution buffer was 1% aqueous ammonia. Default protocol values were used for phosphopeptide enrichment. Enriched samples were directly eluted from AssayMAP Fe(III)-NTA cartridges into a PCR plate containing 20 µL 10% formic acid and 6 ul 0.02% n-dodecyl β-D-maltoside. Samples were then dried in a vacuum centrifuge and reconstituted in 12 µL of 3% acetonitrile + 0.1% FA prior to LC-MS/MS analysis.

For phosphoproteomics data, IMAC enriched fractions were searched as described above with the addition of dynamic phosphorylation (+79.9663 Da) modification on Ser, Thr, or Tyr residues. Top-scoring assignments for phosphorylation site localization were reported after further processing the phospho-proteomics data using the Ascore algorithm.[32,33] False discovery rate (FDR) calculation was performed using a reversed sequence decoy database approach and results were then filtered to a 1% FDR at the unique protein and peptide level. Parsimonious inference was applied to eliminate redundancy in peptide-to-protein mapping.[34] Proteins and phosphosites were also required to be quantified in at least half of samples. After applying these filters, we obtained 9,013 proteins and 29,545 phosphosites detected in at least 50% of the six MPNST PDXs with two technical replicates each. After normalizing to the pooled reference channel, values were median normalized across samples and features. Proteomics data can be found in Tables S1 and S2.

Characterization of molecular signatures correlated to chr8q status

We ranked molecular features based on the correlation between their relative expression and median chr8q copy number of the biological sample as described in **Figure 1A**. Copy number data, depicted in **Figure 1B**, was derived from our previous work [8] and genes were identified as belonging to chr8q using the positional gene set available from the Molecular Signatures Database (MSigDB, https://www.gsea-msigdb.org/gsea/msigdb/index.jsp)[35] accessed using the function msigdbr from the msigdbr R package as shown in **Figure 1C**[36]. We performed Spearman correlations between median chr8q copy number and normalized expression values for MPNST PDXs using the function cor.test from the stats R package (http://www.R-project.org/)[37], requiring at least six samples per correlation. P-values were adjusted using the Benjamini-Hochberg procedure [38] with the function qvalue from the qvalue R package [39]. Molecular features were then considered significantly correlated with chr8q median copy number if their adjusted p-value was less than or equal to a threshold of 0.05 (shaded values in Figure 1C). We then imposed an additional filter requiring correlated features to have a Spearman rank correlation >0.75 or less than -0.75 (dashed line Figure 1C). Out of 69,797 genes from copy number data, 1,630 out of 19,208

genes from the RNA-Seq data, 208 out of 9,013 proteins and 439 out of 28,866 phospho-sites met these criteria (**Figure 1D-E**).

Gene set enrichment analysis

To examine global trends in expression correlated with chr8q median copy number, we performed gene set enrichment analysis (GSEA).[40] Specifically, we input Spearman correlation estimates from our molecular signature of chr8q gain (described above) into GSEA and calculated the enrichment of gene sets available in the Hallmarks gene list, positional gene list, and Transcription Factor Targets (GTRD) collections on the Molecular Signatures Database (MSigDB, https://www.gsea-msigdb.org/gsea/msigdb/index.jsp)[35] accessed using the function msigdbr from the msigdbr R package.[36] Due to a high percentage of ties in our input rank lists (88-98%; Fig. S1), we permuted tied features (1,000 permutations to generate an ES_ties distribution) in addition to the standard practice of permuting set annotations (another 1,000 permutations to generate an ES_null distribution). We then calculated p-values using the weakest enrichment score (i.e., ES_min) from these tie permutations. We also take a conservative approach for the false discovery rate (FDR) q-values by using the NES_min to identify the fractions of stronger same-signed NES_null and NES_max (i.e., strongest possible scores from other gene sets). Finally, the ES is taken as the mean of the ES_ties distribution and, as standard, the NES is defined as the ES divided by the mean of same-signed ES_null values.

To evaluate the robustness of this adapted GSEA approach which accounts for ties, we: (1) confirmed that chr8q was enriched with chr8q gain as expected (**Figure 1F**) and (2) performed a simulation study (Fig. S2). Specifically, we used the 9,013 gene symbols from our global proteomics correlation analysis and generated a representative normal distribution based on that of the real data (normal distribution centered around 0 with standard deviation of 0.5, maximum absolute value of 1, and a median of 90 ties per rank value). Next, we used the MSigDB Hallmark gene set collection of 50 gene sets and added one synthetic gene set consisting of randomly sampled genes from our input list of 9,013. To test the effect of the gene set size on the enrichment, the size of this synthetic gene set was varied from 30 to 300. Once the synthetic gene set was randomly selected, the distribution of the genes in this synthetic gene set was shifted up or down by up to 0.25. This process was repeated a total of 20 times to assess reproducibility. The further this synthetic gene set was shifted, the stronger the enrichment score and more significant the enrichment. However, with no shift (i.e., no difference in distributions between the gene set and the rest of the genes), there were no significant enrichments (i.e., no false discovery), assuring us that this adapted GSEA approach with a distribution is robust even with a highly tied distribution like those of our correlation estimates. We ran the GSEA with simulation on the Hallmarks and transcription factor gene sets and used a p-value cutoff of 0.05 and FDR cutoff of 0.25. 25 of the 28 enriched pathways are depicted in Figure 2A and 25 of the 264 enriched transcription factors in Figure 2B.

Kinase enrichment analysis

To identify kinases which may be differentially active based on chr8 median copy number, we used the kinase-substrate database from PhosphoSitePlus[41] to perform enrichment analysis. The database was downloaded on November 1, 2023. Kinases with at least 6 substrates quantified were evaluated based on enrichment of phospho-site correlations with median chr8q copy number. Kinases with negative enrichments are predicted to be less active with higher chr8q copy number. We used a significance filter of $p < 0.05$ and adjusted p-value < 0.25 to identify 8 out of 182 (4.3%) of kinases as enriched per the recommendation for enrichment analysis as shown in Figure 2C.[40]

Network analysis

To identify potential protein relationships between the features that were correlated with copy number, we built networks from positively and negatively correlated features using the STRING database[42] of physical protein interactions by inputting protein-level features (transcription factors, proteins, and kinases) positively and negatively associated with chr8q copy number, respectively. This approach acts as reinforcement for the enrichment statistics, which can vary across runs due to the stochastic nature of the NES calculation. For the transcription factor and kinase analysis highlighted in Figure 2, this included 260 transcription factors and 5 kinases (PDHK3, CAMK1D, TLK1, MAK, and MAPK12) which were predicted to be more active with higher chr8q copy number or 2 transcription factors (TFAM and HMCES) and 3 kinases (NEK1, MOK, PRKG2) which were predicted to be less active with higher chr8q copy number. For Figure 3, 101 proteins with expression significantly positively or 107 negatively correlated with median chr8q copy number were added to either the positive or negative networks assembled for Figure 2, respectively. Networks were assembled using igraph[43] and then visualized in Cytoscape[44] using RCy3 as depicted in Figure 2D-E.[45] Centrality was calculated using the eigen_centrality function available in the igraph R package.

Drug mechanism enrichment analysis

To identify drug mechanisms of action which may be selectively toxic to MPNSTs based on chr8q copy number, we performed drug mechanism enrichment analysis (DMEA).[46] In particular, we input Spearman correlation estimates from our molecular signature of chr8q gain (described above) and queried Cancer Cell Line Encyclopedia (CCLE) global proteomics[47] and RNA-Seq[48] datasets such that the cancer cell lines were ranked based on similarity to our input proteomics and transcriptomics signatures of chr8q gain, respectively. Next, we queried the Profiling Relative Inhibition Simultaneously in Mixtures (PRISM) drug screen[17] to rank 1,448 drugs based on Pearson correlations between drug sensitivity scores (Area Under the Curve, AUC) and these similarity scores in up to 327 adherent cancer cell lines. Finally, we evaluated the enrichment of drugs grouped by 83 known mechanisms of action annotations available from the PRISM drug screen database represented in this drug rank list. P-values and FDR q-values were

calculated using 1,000 permutations and a minimum of 6 drugs were required per mechanism of action set. Per the recommendations for DMEA[46] and enrichment analysis in general,[40] we used a p-value cutoff of 0.05 and FDR cutoff of 0.25. Significant mechanisms are depicted in Fig. 3A, while individual drugs are in Fig. 3B-C.

Cell lines and reagents

Four patient-derived NF1-MPNST cell lines (JH-2-002, JH-2-055d, JH-2-079c, and JH-2-103)[18] were generated in our laboratories at Johns Hopkins University (JH; Baltimore, MD, USA) from biospecimens collected during surgical resection from patients with NF1.[9,11] Material was collected under the Institutional Review Board–approved protocol, and all patients provided written informed consent. STS26T, ST8814 and NF90.8 cell lines were from Dr. Gregory Riggins (JH; Baltimore, MD, USA). S462 cell line was provided by Dr. Peter Houghton (UT Health San Antonio, TX, USA). NF10.1, NF11.1 were provided by Dr. Margaret Wallace (University of Florida; Gainesville, FL, USA). All cell lines used in these experiments were verified by short-tandem repeat (STR) profiling for cell line authentication at Johns Hopkins University Core Facility, tested negative for mycoplasma contamination, and passaged *in vitro* for fewer than three months after resuscitation. All growth media were supplemented with 10% FBS, 2 mmol/L L-glutamine, and 1% penicillin–streptomycin.

Erlotinib, osimertinib, and volasertib were purchased from MedChemExpress (Monmouth Junction, NJ, USA). BI-2536 was obtained from opnMe by Boehringer Ingelheim. Drugs for *in vitro* studies were dissolved in DMSO to yield 10 or 1 mmol/L stock solutions and stored at −20°C.

Fluorescence in situ hybridization

Fluorescence *in situ* hybridization (FISH) was performed on nine MPNST cell lines at the Johns Hopkins Cancer Center Cytogenetics Core Facility. 100 interphase nuclei were scored after FISH with a tri-color probe, where green signal corresponded to *IGH* (located on chr14q32), red corresponded to *MYC* (located on chr8q24), and aqua corresponded to CEP8 (chromosome enumeration probe for the centromere of chr8). Images are depicted in Figure 4A. Gain was defined as three or more copies in at least 50% of cells, summarized in Figure 4B-C.

Cell proliferation assay

JH-2-055d cells were seeded in 96-well plates at 7500 cells per well and other cell lines at 1000-2000 cells per well. A dose range of the compounds indicated was prepared by serial dilutions and then added to the wells containing adherent cells. Cells were incubated with drugs for five days. Cell growth was quantitated using the Cell Counting Kit-8 (Dojindo; Rockville, MD, USA) assay. For each cell line, two to four biological replicates with three to four technical replicates of each condition were measured.

Relative survival in the presence of drugs was normalized to the untreated controls after background subtraction and plotted as a function of $\log_{10}$ transformed drug doses. The model Sigmoidal dose-response was used to perform the non-linear curve fitting and interpolate the IC50 values using the GraphPad Prism 10. Results and summary statistics are depicted in Figure 5.

Discussion

Here we demonstrate that chr8q gain is observed at various levels in MPNST patient-derived xenografts and is associated with changes in levels of RNA and protein expression as well as phosphorylation. Specifically, we used our established cohort of MPNST PDX and associated copy number data to identify genes and proteins that are correlated with chr8q gain (Fig. 1). We also identified pathway level changes including increased MYC activity with chr8q gain and differential activity of transcription factors and kinases (Fig. 2). We used these data to identify putative drug targets to selectively target chr8q gain vs. diploid MPNST populations (Fig. 3) and validated these across a suite of genomically diverse cell lines (Fig. 4-5). These analyses provide unique insight into the distinct signaling activity within both chr8q diploid tumor populations as well as those with chr8q gain.

Not unexpectedly, MYC was identified as the prominent driver mediating signaling changes associated with chr8q gain, both at the mRNA and protein levels (Fig. 1). This finding was not surprising, given the fact that *MYC* is located on chr8q itself [15] and is a known oncogene.[49] However, our analysis identified many other genes that are associated with chr8q gain but are not physically located on chr8q, and also found significant depletion of chr8p23 in samples with high chr8q copy number (Fig. 1F) suggesting that chr8p and chr8q may be differentially regulated in MPNST. These findings align with previous studies that show both chr8p deletion and chr8q gain are associated with tumor proliferation.[50]

Additionally, our multi-omics analysis was able to identify PLK and EGFR inhibitors as selectively effective against MPNSTs that are chr8q gain or diploid, respectively. This result was consistent across the cell line correlation data (Fig. 3A-C) as well as network analysis (Fig. 3D-E). Our proteogenomic data analysis revealed that chr8q gain MPNST tumors display significant upregulation of cell proliferation and cell cycle progression, evidenced by the positive enrichment of MYC targets, E2F targets and G2M checkpoint pathways at both the RNA and protein levels (Fig. 2C). PLK1 functions downstream of RTK/MEK/ERK signaling, as the master orchestrator of the mitosis phase of cell cycle and has emerged as a promising target for MPNST.[51–53] PLK1 inhibitors have been found to inhibit MYC activity[54] and we have now shown that they demonstrate selectivity for *MYC* gain MPNST (Fig. 5A,C). In the absence of *MYC* gain, chr8q diploid MPNST may be forced to rely heavily on upstream RTK/MEK/ERK pathways for cell survival and proliferation. The ErbB receptor family constitutes a major RTK pathway and specifically, EGFR has been found to promote MPNST transformation via phosphorylation of STAT3.[25] The differential response to PLK1 and EGFR inhibitors observed in these MPNSTs illustrates the importance of considering chr8q status in future MPNST studies.

One limitation of this study that is unavoidable in rare tumors is sample size. With a low sample size, one outlier sample can have a strong effect on correlation estimates. We attempted to mitigate this concern by using Spearman rank-based estimates and permuting tied features for enrichment analyses, though this still caused variation, necessitating network analysis to confirm top hits. We also only had one MPNST PDX in our proteomics study (WU-225) with TP53 loss of function, which is notable since phosphorylation of TP53BP1 contributed to the NEK1 kinase enrichment result (Fig. S3). For our viability assay to test the selective efficacy of PLK1 and EGFR inhibitors, we also only had one *MYC*-diploid MPNST cell line (JH-2-055d) to compare against eight *MYC*-gain lines. This limitation is also difficult to avoid given that our previous study demonstrated that 80% of MPNST harbor highly recurrent chr8q gain.[8] Though our computational analysis included 1,448 drugs spanning 83 drug mechanisms of action screened in 327 adherent cancer cell lines, our drug sensitivity predictions were restricted to these drugs already tested in pan-cancer cell lines, none of which were labeled as MPNST cell lines. Additionally, cell line behavior may differ from that of the patient tumor from which the cell line was derived.

Overall, this study serves as a multi-omics resource on MPNST patient-derived xenografts and leverages these data to identify dramatic changes in expression, pathway activity, and drug sensitivity based on chr8q status. This is a crucial step towards stratifying drug treatments for each patient with MPNST based on *MYC* copy number as well as providing a way to treat distinct sub-populations within a tumor that might have both chr8q gain cells and chr8q diploid cells. PLK1 and EGFR inhibitors merit further evaluation in *MYC*-gain and -diploid MPNSTs, respectively. Further interrogating the selectivity of these inhibitors for MPNSTs based on *MYC* status and testing PLK1 and EGFR inhibitors in combination will also be important for targeting tumor heterogeneity, considering both chr8q-gain and -diploid cancer cells may be found in any given tumor.

Declarations

Data availability

Data are available upon request on Synapse at https://synapse.org/chr8_mpnst.

Code availability

Processing scripts are publicly available on GitHub at https://github.com/PNNL-CompBio/MPNST_chr8/.

Acknowledgements

This work was funded by the United States Department of Defense Office of the Congressionally Directed Medical Research Programs (CDMRP) Neurofibromatosis Research Program (NFRP) under W81XWH-22-1-0324 awarded to ACH and HT9425-23-1-0253 awarded to ACH, SJCG, DAL, CAP, and DKW. The mass spectrometry work was performed at the Environmental Molecular Sciences Laboratory,

a U.S. Department of Energy National Scientific User Facility located at the Pacific Northwest National Laboratory operated under contract DE-AC05-76RL01830.

Author contributions

A.C.H. and S.J.C.G. conceived of the study. S.A. and G.O. generated proteomics samples. C.H., M.A.G., and P.D.P. generated the proteomics data. B.B.G. processed the proteomics data, integrated and analyzed the multi-omics data sets, and led the writing of the manuscript. S.J.C.G. formatted the analysis code for publication and re-use. J.W. performed cell viability experiments and preprocessed samples for FISH. Y.Z. performed analysis on FISH. All authors advised on the study and reviewed the manuscript.

Competing interests

Dr. Hirbe has served on advisory boards for Alexion, Springworks, and Aadi Biosciences. The other authors declare no competing interests.

References

1. Larsson, A. T. *et al.* Ex vivo to in vivo model of malignant peripheral nerve sheath tumors for precision oncology. *Neuro-Oncol.* **25**, 2044–2057 (2023).
2. Sobczuk, P. *et al.* Systemic Treatment for Advanced and Metastatic Malignant Peripheral Nerve Sheath Tumors-A Sarcoma Reference Center Experience. *J. Clin. Med.* **9**, 3157 (2020).
3. Akshintala, S. *et al.* Outcome of Patients With Malignant Peripheral Nerve Sheath Tumors Enrolled on Sarcoma Alliance for Research Through Collaboration (SARC) Phase II Trials. *The Oncologist* **28**, 453–459 (2023).
4. Reilly, K. M. *et al.* Neurofibromatosis Type 1-Associated MPNST State of the Science: Outlining a Research Agenda for the Future. *J. Natl. Cancer Inst.* **109**, djx124 (2017).
5. Hirbe, A. C. *et al.* Contemporary Approach to Neurofibromatosis Type 1-Associated Malignant Peripheral Nerve Sheath Tumors. *Am. Soc. Clin. Oncol. Educ. Book Am. Soc. Clin. Oncol. Annu. Meet.* **44**, e432242 (2024).
6. Cortes-Ciriano, I. *et al.* Genomic Patterns of Malignant Peripheral Nerve Sheath Tumor (MPNST) Evolution Correlate with Clinical Outcome and Are Detectable in Cell-Free DNA. *Cancer Discov.* **13**, 654–671 (2023).
7. Zhang, M. *et al.* Somatic mutations of SUZ12 in malignant peripheral nerve sheath tumors. *Nat. Genet.* **46**, 1170–1172 (2014).

8. Dehner, C. *et al.* Chromosome 8 gain is associated with high-grade transformation in MPNST. *JCI Insight* **6**, e146351, 146351 (2021).
9. Pollard, K. *et al.* A clinically and genomically annotated nerve sheath tumor biospecimen repository. *Sci. Data* **7**, 184 (2020).
10. Wang, J., Pollard, K., Calizo, A. & Pratilas, C. A. Activation of Receptor Tyrosine Kinases Mediates Acquired Resistance to MEK Inhibition in Malignant Peripheral Nerve Sheath Tumors. *Cancer Res.* **81**, 747–762 (2021).
11. Banerjee, J. *et al.* Integrated genomic analysis of NF1-associated peripheral nerve sheath tumors: an updated biorepository dataset. *Sci. Data* **12**, 1229 (2025).
12. Lin, C. Y. *et al.* Transcriptional Amplification in Tumor Cells with Elevated c-Myc. *Cell* **151**, 56–67 (2012).
13. Zhakula-Kostadinova, N. & Taylor, A. M. Patterns of Aneuploidy and Signaling Consequences in Cancer. *Cancer Res.* **84**, 2575–2587 (2024).
14. Subramanian, A. *et al.* Gene set enrichment analysis: a knowledge-based approach for interpreting genome-wide expression profiles. *Proc. Natl. Acad. Sci. U. S. A.* **102**, 15545–15550 (2005).
15. Seal, R. L. *et al.* Genenames.org: the HGNC resources in 2023. *Nucleic Acids Res.* **51**, D1003–D1009 (2023).
16. Szklarczyk, D. *et al.* The STRING database in 2025: protein networks with directionality of regulation. *Nucleic Acids Res.* **53**, D730–D737 (2024).
17. Corsello, S. M. *et al.* Discovering the anti-cancer potential of non-oncology drugs by systematic viability profiling. *Nat. Cancer* **1**, 235–248 (2020).
18. Wang, J. *et al.* CDK4/6 inhibition enhances SHP2 inhibitor efficacy and is dependent upon RB function in malignant peripheral nerve sheath tumors. *Sci. Adv.* **9**, eadg8876 (2023).
19. Erlichman, C. *et al.* Phase I study of EKB-569, an irreversible inhibitor of the epidermal growth factor receptor, in patients with advanced solid tumors. *J. Clin. Oncol. Off. J. Am. Soc. Clin. Oncol.* **24**, 2252–2260 (2006).
20. Bryce, A. H. *et al.* Phase I study of temsirolimus in combination with EKB-569 in patients with advanced solid tumors. *Invest. New Drugs* **30**, 1934–1941 (2012).
21. Le, X. *et al.* Poziotinib for EGFR exon 20-insertion NSCLC: Clinical efficacy of the phase 2 ZENITH trial and differential impact of EGFR exon 20 insertion location on sensitivity. *Nat. Commun.* **16**, 8358 (2025).
22. Elamin, Y. Y. *et al.* Poziotinib for Patients With HER2 Exon 20 Mutant Non-Small-Cell Lung Cancer: Results From a Phase II Trial. *J. Clin. Oncol. Off. J. Am. Soc. Clin. Oncol.* **40**, 702–709 (2022).
23. Perry, A. *et al.* Differential NF1, p16, and EGFR patterns by interphase cytogenetics (FISH) in malignant peripheral nerve sheath tumor (MPNST) and morphologically similar spindle cell neoplasms. *J. Neuropathol. Exp. Neurol.* **61**, 702–709 (2002).

24. Keizman, D. *et al.* Expression and significance of EGFR in malignant peripheral nerve sheath tumor. *J. Neurooncol.* **94**, 383–388 (2009).
25. Wu, J. *et al.* EGFR-STAT3 signaling promotes formation of malignant peripheral nerve sheath tumors. *Oncogene* **33**, 173–180 (2014).
26. Pino, J. C. *et al.* Mapping the proteogenomic landscape enables prediction of drug response in acute myeloid leukemia. *Cell Rep. Med.* **5**, 101359 (2024).
27. Krug, K. *et al.* Proteogenomic Landscape of Breast Cancer Tumorigenesis and Targeted Therapy. *Cell* **183**, 1436-1456.e31 (2020).
28. Mertins, P. *et al.* Reproducible workflow for multiplexed deep-scale proteome and phosphoproteome analysis of tumor tissues by liquid chromatography-mass spectrometry. *Nat. Protoc.* **13**, 1632–1661 (2018).
29. Huang, C. *et al.* Proteogenomic insights into the biology and treatment of HPV-negative head and neck squamous cell carcinoma. *Cancer Cell* **39**, 361-379.e16 (2021).
30. Clark, D. J. *et al.* Integrated Proteogenomic Characterization of Clear Cell Renal Cell Carcinoma. *Cell* **179**, 964-983.e31 (2019).
31. Hu, Y. *et al.* Integrated Proteomic and Glycoproteomic Characterization of Human High-Grade Serous Ovarian Carcinoma. *Cell Rep.* **33**, 108276 (2020).
32. Gassaway, B. M. *et al.* A multi-purpose, regenerable, proteome-scale, human phosphoserine resource for phosphoproteomics. *Nat. Methods* **19**, 1371–1375 (2022).
33. Beausoleil, S. A., Villén, J., Gerber, S. A., Rush, J. & Gygi, S. P. A probability-based approach for high-throughput protein phosphorylation analysis and site localization. *Nat. Biotechnol.* **24**, 1285–1292 (2006).
34. Zhang, B., Chambers, M. C. & Tabb, D. L. Proteomic parsimony through bipartite graph analysis improves accuracy and transparency. *J. Proteome Res.* **6**, 3549–3557 (2007).
35. Liberzon, A. *et al.* Molecular signatures database (MSigDB) 3.0. *Bioinformatics* **27**, 1739–1740 (2011).
36. Dolgalev, I. msigdbr: MSigDB Gene Sets for Multiple Organisms in a Tidy Data Format. 25.1.1 https://doi.org/10.32614/CRAN.package.msigdbr (2018).
37. *R a Language and Environment for Statistical Computing: Reference Index*. (R Foundation for Statistical Computing, Vienna, 2010).
38. Benjamini, Y. & Hochberg, Y. Controlling the False Discovery Rate: A Practical and Powerful Approach to Multiple Testing. *J. R. Stat. Soc. Ser. B Methodol.* **57**, 289–300 (1995).
39. John D. Storey With Contributions From Andrew J. Bass, A. qvalue. Bioconductor https://doi.org/10.18129/B9.BIOC.QVALUE (2017).
40. Subramanian, A. *et al.* Gene set enrichment analysis: a knowledge-based approach for interpreting genome-wide expression profiles. *Proc. Natl. Acad. Sci. U. S. A.* **102**, 15545–15550 (2005).

41. Hornbeck, P. V. *et al.* PhosphoSitePlus, 2014: mutations, PTMs and recalibrations. *Nucleic Acids Res.* **43**, D512-520 (2015).
42. Szklarczyk, D. *et al.* The STRING database in 2023: protein-protein association networks and functional enrichment analyses for any sequenced genome of interest. *Nucleic Acids Res.* **51**, D638–D646 (2023).
43. Csárdi, G. *et al.* igraph for R: R interface of the igraph library for graph theory and network analysis. Zenodo https://doi.org/10.5281/ZENODO.7682609 (2025).
44. Shannon, P. *et al.* Cytoscape: a software environment for integrated models of biomolecular interaction networks. *Genome Res.* **13**, 2498–2504 (2003).
45. Gustavsen, J. A., Pai, S., Isserlin, R., Demchak, B. & Pico, A. R. RCy3: Network biology using Cytoscape from within R. *F1000Research* **8**, 1774 (2019).
46. Garana, B. B., Joly, J. H., Delfarah, A., Hong, H. & Graham, N. A. Drug mechanism enrichment analysis improves prioritization of therapeutics for repurposing. *BMC Bioinformatics* **24**, 215 (2023).
47. Nusinow, D. P. *et al.* Quantitative Proteomics of the Cancer Cell Line Encyclopedia. *Cell* **180**, 387-402.e16 (2020).
48. Ghandi, M. *et al.* Next-generation characterization of the Cancer Cell Line Encyclopedia. *Nature* **569**, 503–508 (2019).
49. Dhanasekaran, R. *et al.* The MYC oncogene — the grand orchestrator of cancer growth and immune evasion. *Nat. Rev. Clin. Oncol.* **19**, 23–36 (2022).
50. Zhakula-Kostadinova, N. & Taylor, A. M. Patterns of Aneuploidy and Signaling Consequences in Cancer. *Cancer Res.* **84**, 2575–2587 (2024).
51. Nair, J. S. & Schwartz, G. K. Inhibition of polo like kinase 1 in sarcomas induces apoptosis that is dependent on Mcl-1 suppression. *Cell Cycle Georget. Tex* **14**, 3101–3111 (2015).
52. Kolberg, M. *et al.* Drug sensitivity and resistance testing identifies PLK1 inhibitors and gemcitabine as potent drugs for malignant peripheral nerve sheath tumors. *Mol. Oncol.* **11**, 1156–1171 (2017).
53. Guo, J. *et al.* Polo-like kinase 1 as a therapeutic target for malignant peripheral nerve sheath tumors (MPNST) and schwannomas. *Am. J. Cancer Res.* **10**, 856–869 (2020).
54. Xiao, D. *et al.* Polo-like Kinase-1 Regulates Myc Stabilization and Activates a Feedforward Circuit Promoting Tumor Cell Survival. *Mol. Cell* **64**, 493–506 (2016).

Figures

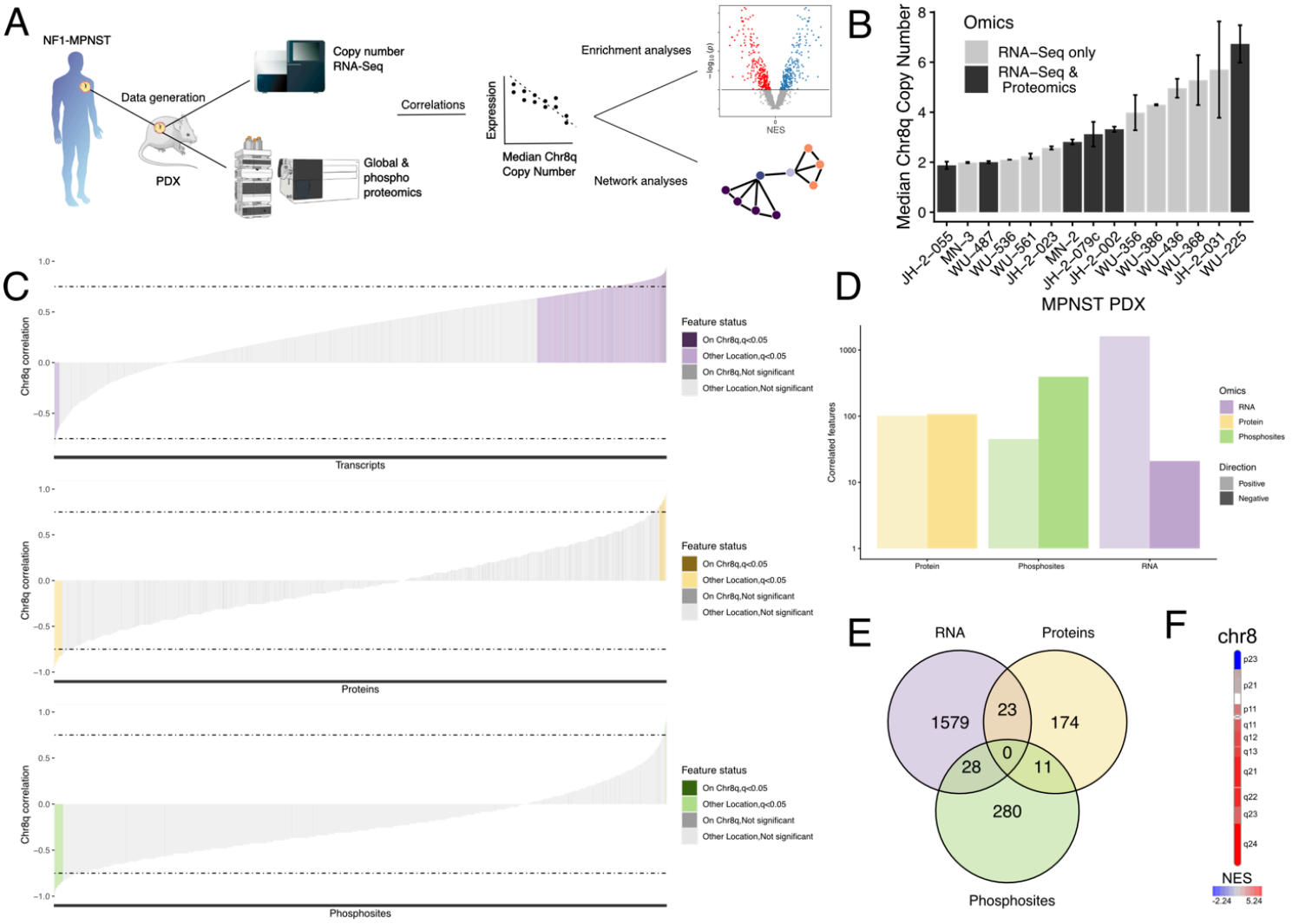


Figure 1

Multi-omics analysis of chr8q gain

(**A**) Overview of the experimental approach. LC-MS proteomics was performed on six of sixteen MPNST PDX samples with RNA-Seq and copy number data with two technical replicates each. Downstream analyses included correlation with chr8q status followed pathway enrichment using rank statistics, and network analyses. **(B)**Median chr8q copy number of the samples used in this study. Bar colors indicate which data are available for each PDX. (**C**) Correlation of each feature with chr8q copy number. Statistically significant correlations are shaded, while dashed lines indicate the cut-off of 0.75 or -0.75 used to determine biological significance. (**D**) Number of features significantly positively or negatively correlated with median chr8q copy number across RNA-Seq (RNA) and LC-MS/MS proteomics (protein) and phosphoproteomics levels (adjusted p-value < 0.05). (**E**) Overlap of genes significantly correlated across RNA, protein, and phosphoproteomic measurements. (**F**) Normalized enrichment scores (NES) of chr8 segments based on correlation of copy number with median chr8q copy number confirms the ability to identify chr8q amplification using rank-based enrichment statistics.

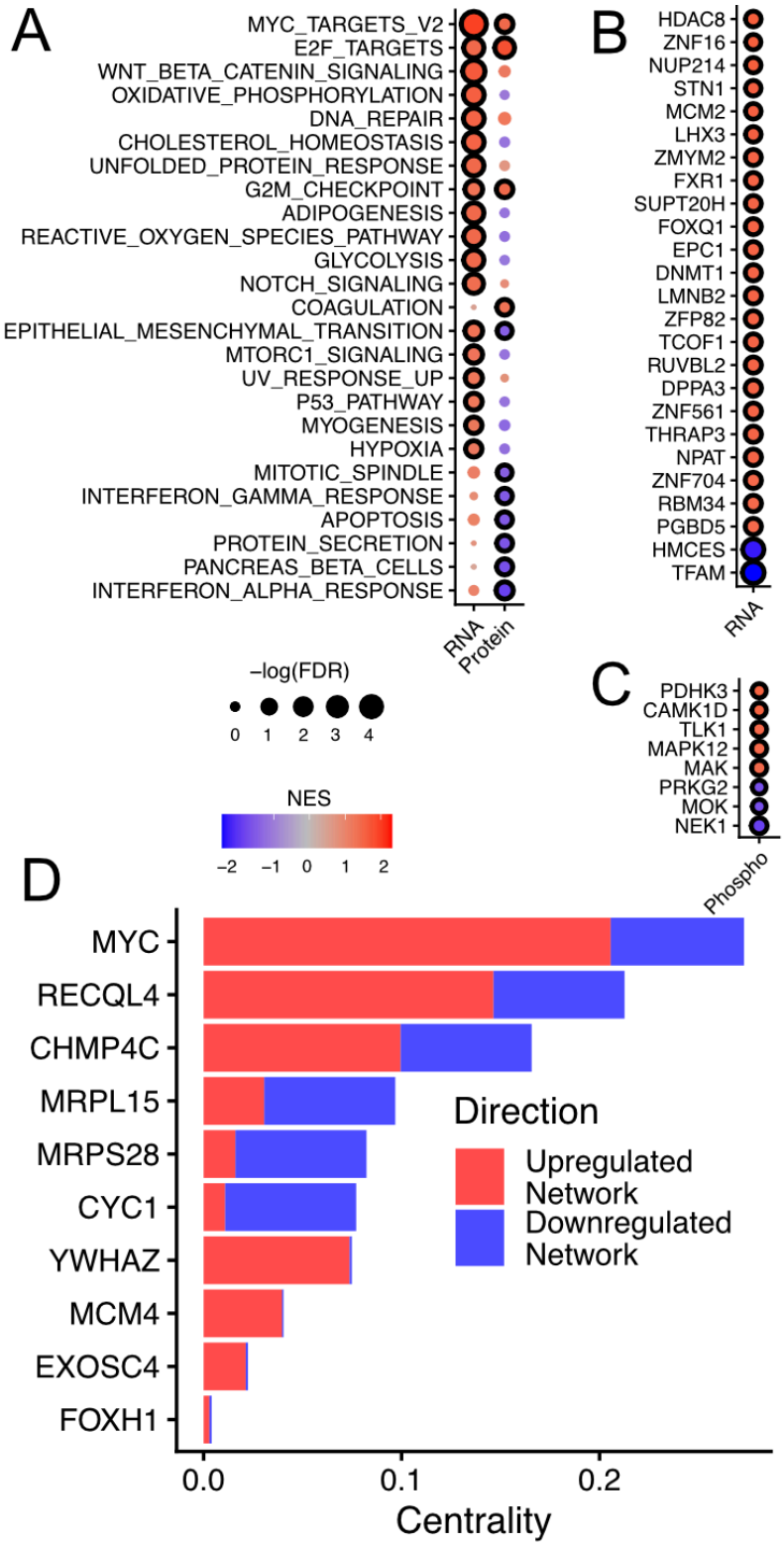


Figure 2

Pathway-level changes caused by chr8q gain measured at transcriptional and post-transcriptional levels Enrichment based on correlations with median chr8q copy number using either (**A**) Hallmark gene sets from MSigDB across RNA-Seq (RNA) and LC-MS/MS proteomics (protein) levels, (**B**) transcription factor targets from MSigDB for RNA, or (**C**) the kinase-substrate database from PhosphoSite Plus with phosphosite data from LC-MS/MS proteomics. Circle with a border: significant enrichments ($p < 0.05$ &

FDR < 0.25). (**D**) Chr8q gene-associated proteins appearing in both up- and down-regulated networks of transcription factors and kinases ranked by mean centrality.

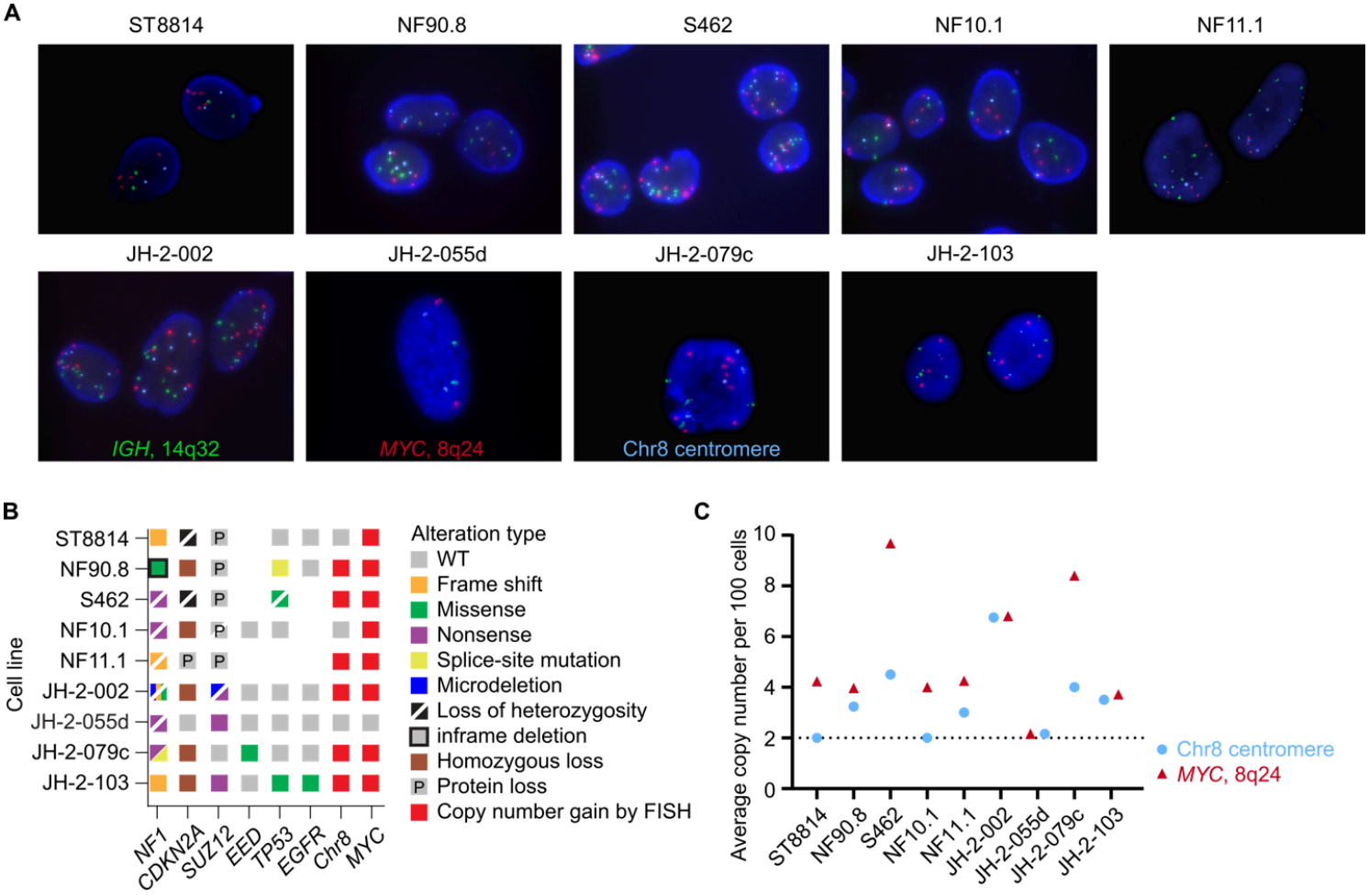


Figure 3

Drug sensitivity analysis reveals potential targets based on chr8q status

(**A**) Enriched drug mechanism sets where NES < 0 indicate potential selective toxicity to MPNSTs with chr8q gain and vice-versa. FDR: false discovery rate. NES: normalized enrichment score. Circled with a border: significant enrichments ($p < 0.05$ & FDR < 0.25). (**B**) Top five significantly correlated drugs based on absolute Pearson correlation estimates using RNA. (C) Top significantly correlated drugs based on protein data. (**D**) Physical interactions found in STRING database between EGFR, MYC, and proteins up-regulated with higher median chr8q copy number, (E) Physical interactions found in STRING database between PLK1, MYC, and proteins down-regulated with higher median chr8q copy number

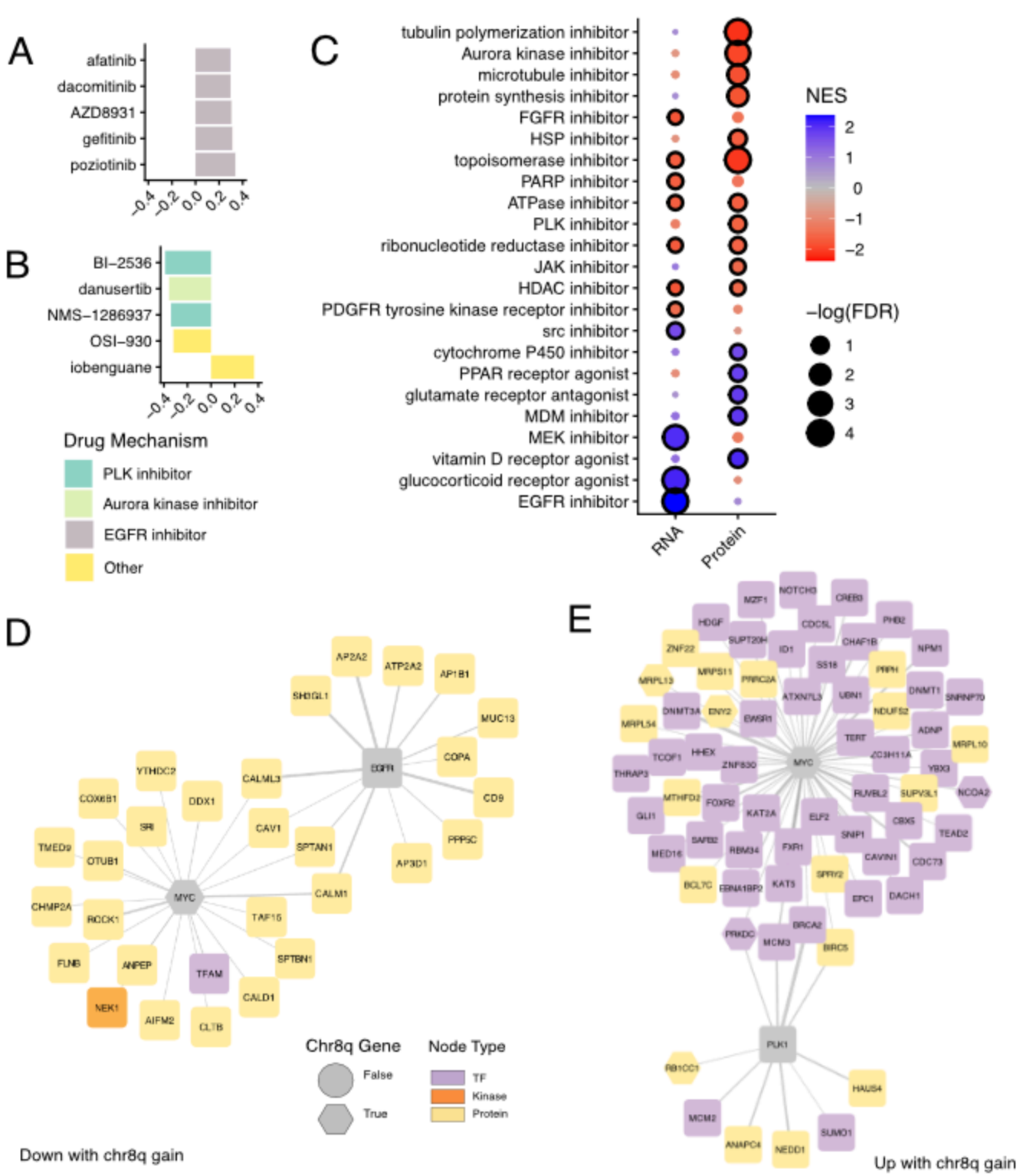


Figure 4

FISH determines chr8 and *MYC* copy number of NF1-MPNST cell lines

(A) Representative images of FISH in nine NF1-MPNST cell lines displaying aqua signal for the centromere of chr8, red signal for MYC/8q24, and green signal for IGH/14q32. (B) OncoPrint integrating key genomic driver features in nine NF1-MPNST cell lines, combining data from our previous study[18]

with the FISH findings of the current work. (C) Average copy numbers of MYC or chr8 were quantified per 100 interphase cells in the FISH experiment.

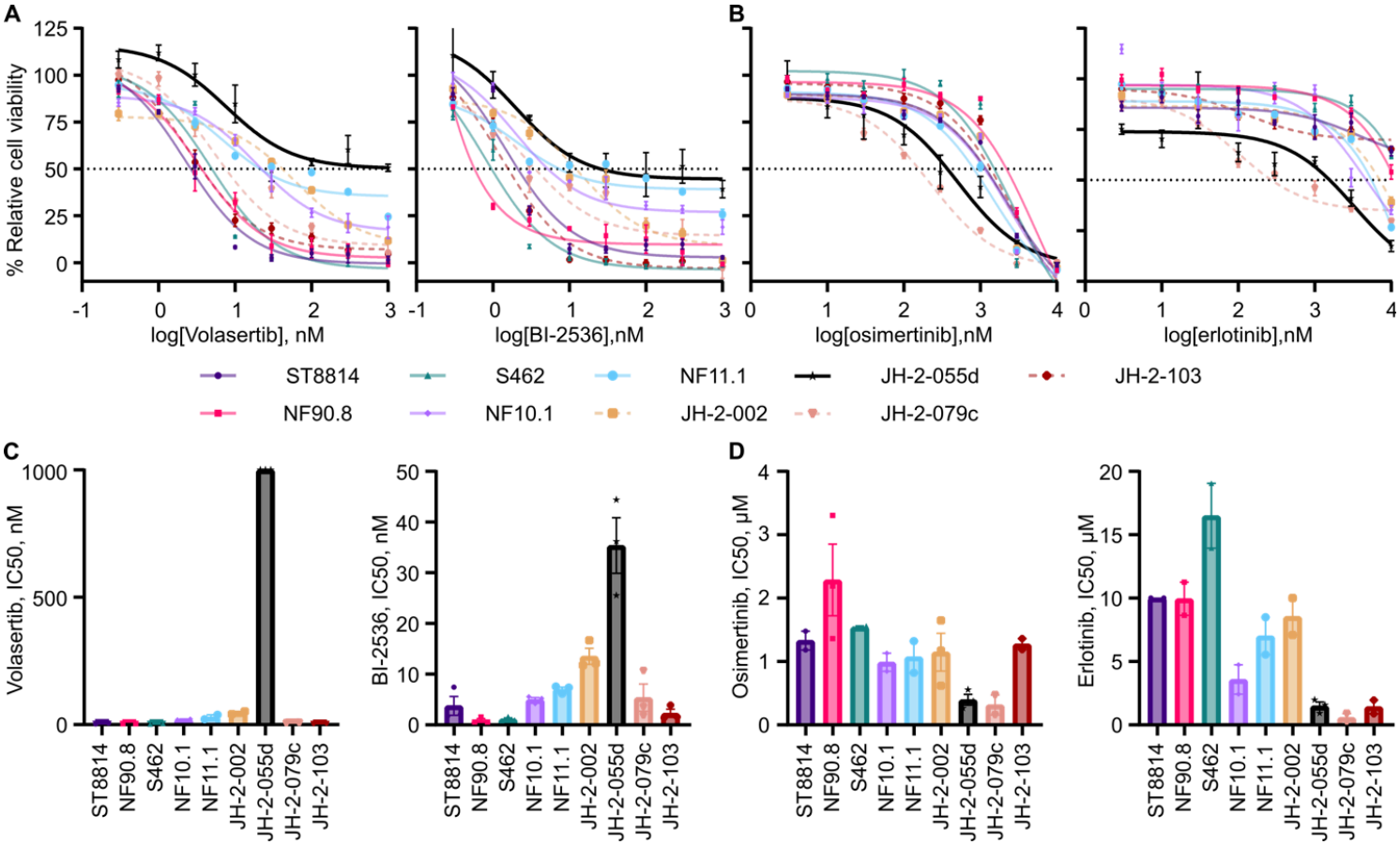


Figure 5

MPNST cell lines have differential response to PLK1 and EGFR inhibitors

(**A-B**) Percent relative cell viability and (**C-D**) IC50 values of MPNST cell lines after 5 days of treatment with either PLK1 inhibitors volasertib or BI-2536 (**A** & **C**) or EGFR inhibitors erlotinib or osimertinib (**B** & **D**).

Supplementary Files

This is a list of supplementary files associated with this preprint. Click to download.

- SupplementaryTable8FISH.doc
- SupplementaryTable4GSEA.xlsx
- SupplementaryTable5KSEA.xlsx
- figS3.png
- FigS1.png
- SupplementaryTable7DMEA.xlsx

- SuppFig220241217.png
- SupplementaryTable1global.xlsx
- SupplementaryTable2phospho.xlsx
- SupplementaryTable6Networkanalyses.xlsx
- SupplementaryTable3Correlations.xlsx